

Multiparameter hierarchical sensitivity analysis of tilt-to-length coupling noise in Taiji science interferometer

Fei Xie(谢菲), Xiaodong Peng(彭晓东), Wenlin Tang(唐文林), Mengyuan Zhao(赵梦圆), and Xiaoshan Ma(马晓珊)

Citation: Chin. Phys. B, 2026, 35 (**1**): 010701. DOI: 10.1088/1674-1056/ae07a8
http://cpb.iphy.ac.cn; http://iopscience.iop.org/cpb

What follows is a list of articles you may be interested in

Doppler radial velocity detection based on Doppler asymmetric spatial heterodyne spectroscopy technique for absorption lines

Yin-Li Kuang(况银丽), Liang Fang(方亮), Xiang Peng(彭翔), Xin Cheng(程欣), Hui Zhang(张辉), En-Hai Liu(刘恩海)
Chin. Phys. B, 2020, 29 (**2**): 020701. DOI: 10.1088/1674-1056/ab5fc3

Negativity of Wigner function and phase sensitivity of an SU(1,1) interferometer

Chun-Li Liu(刘春丽), Li-Li Guo(郭丽丽), Zhi-Ming Zhang(张智明), Ya-Fei Yu(於亚飞)
Chin. Phys. B, 2019, 28 (**6**): 060704. DOI: 10.1088/1674-1056/28/6/060704

An improved arctangent algorithm based on phase-locked loop for heterodyne detection system

Chun-Hui Yan(晏春回), Ting-Feng Wang(王挺峰), Yuan-Yang Li(李远洋), Tao Lv(吕韬), Shi-Song Wu(吴世松)
Chin. Phys. B, 2019, 28 (**3**): 030701. DOI: 10.1088/1674-1056/28/3/030701

Co-focus experiment of segmented mirror

Bin Li(李斌), Wen-Hao Yu(于文豪), Mo Chen(陈莫), Jin-Long Tang(唐金龙), Hao Xian(鲜浩)
Chin. Phys. B, 2017, 26 (**6**): 060706. DOI: 10.1088/1674-1056/26/6/060706

Experimental research on spectrum and imaging of continuous-wave terahertz radiation based on interferometry

Tie-Lin Lu(卢铁林), Hui Yuan(袁 慧), Ling-Qin Kong(孔令琴), Yue-Jin Zhao(赵跃进), Liang-Liang Zhang(张亮亮), Cun-Lin Zhang(张存林)
Chin. Phys. B, 2016, 25 (**8**): 080702. DOI: 10.1088/1674-1056/25/8/080702

Multiparameter hierarchical sensitivity analysis of tilt-to-length coupling noise in Taiji science interferometer

Fei Xie(谢菲)[1,2,3], Xiaodong Peng(彭晓东)[1,2,4,5,†], Wenlin Tang(唐文林)[2], Mengyuan Zhao(赵梦圆)[6], and Xiaoshan Ma(马晓珊)[7,‡]

[1] *School of Fundamental Physics and Mathematical Sciences, Hangzhou Institute for Advanced Study, University of Chinese Academy of Sciences (UCAS), Hangzhou* 310024, *China*

[2] *Key Laboratory of Electronics and Information Technology for Space System, National Space Science Center, Chinese Academy of Sciences (CAS), Beijing* 100190, *China*

[3] *University of Chinese Academy of Sciences, Beijing* 100049, *China*

[4] *Taiji Laboratory for Gravitational Wave Universe, Hangzhou* 310024, *China*

[5] *Key Laboratory of Gravitational Wave Precision Measurement of Zhejiang Province, Hangzhou* 310024, *China*

[6] *School of Information, Xi'an University of Finance and Economics, Xi'an* 710100, *China*

[7] *National Key Laboratory of Science and Technology on Advanced Light-duty Gas-turbine, Institute of Engineering Thermophysics, Chinese Academy of Sciences, Beijing* 100190, *China*

(Received 18 March 2025; revised manuscript received 18 June 2025; accepted manuscript online 17 September 2025)

Tilt-to-length (TTL) coupling noise is a critical issue in space-based gravitational wave detection due to its complex dependence on multiple interacting factors, which complicates the identification of dominant parameters. To address this challenge, we develop a simulation model of the Taiji scientific interferometer, generating noise datasets under multi-parameter conditions. Given the uniqueness of the telescope as well as the convergence behavior of the algorithm, the analysis is structured hierarchically: (i) the telescope level and (ii) the optical bench level. A hierarchical framework combining XGBoost and SHapley Additive exPlanations (SHAP) values is employed to model the intricate relationships between parameters and TTL coupling noise, supplemented by sensitivity analysis. Our results identify pointing jitter and telescope radius as the dominant parameters at the telescope level, while the angles of the plane mirrors and beam splitters are most influential at the optical bench level. The parameter space is reduced from 86 dimensions to 14 dimensions without sacrificing model accuracy. This approach offers actionable insights for optimizing the Taiji interferometer design.

Keywords: space-based gravitational wave detection, intrasatellite science interferometer, tilt-to-length coupling noise, sensitivity analysis

PACS: 07.60.Ly, 04.80.Nn

DOI: 10.1088/1674-1056/ae07a8 **CSTR:** 32038.14.CPB.ae07a8

1. Introduction

Gravitational wave detection serves as a powerful tool for validating Einstein's predictions in general relativity, unveiling extreme astrophysical phenomena, and advancing our understanding of cosmology and new physics.[1–5] Space-based gravitational wave detection, in particular, offers the capability to transcend the constraints of ground-based environments, enabling the effective observation of low-frequency gravitational waves.[6] Gravitational wave detection programs such as the Taiji mission utilize laser interferometry to measure the picometer-level distance variations between two satellite test masses.[4,7] The measurement of the distance between the two test masses is divided into three segments: the distances between each test mass and the local optical benches, measured by the test mass interferometer, and the distance between the two satellites, measured by the scientific interferometer.[8]

Tilt-to-length (TTL) coupling noise arises from the coupling of angular misalignment into the interferometer readout, which is the second largest source of noise in the interferometric measurement system.[9,10] Space-based gravitational wave detection missions such as LISA, Taiji, and TianQin impose stringent requirements on TTL coupling noise, typically at the level of a few picometers per root hertz (pm/Hz$^{1/2}$).[4,5,11] For instance, in the Taiji mission, the allowable contribution from TTL coupling noise must remain below 1 pm/Hz$^{1/2}$, given a total position noise budget of 8 pm/Hz$^{1/2}$.[4] This constraint translates to a laser beam pointing stability requirement of better than 10 nrad/Hz$^{1/2}$. Such tight performance margins underscore the critical importance of accurately modeling and quantitatively evaluating TTL coupling effects. TTL coupling noise affects both the test mass interferometer and the scientific interferometer, with this study focusing specifically on the latter. During spacecraft operations, non-conservative forces induce attitude jitter, leading to pointing errors in the laser beam transmitted from the distant spacecraft relative to the local one.

†Corresponding author. E-mail: Pxd@nssc.ac.cn

‡Corresponding author. E-mail: maxiaoshan@iet.cn

© 2026 Chinese Physical Society and IOP Publishing Ltd. All rights, including for text and data mining, AI training, and similar technologies, are reserved.

This pointing instability is the primary source of TTL coupling noise in the scientific interferometer.[12] In addition, imperfections in the telescope optics, which introduce wavefront aberrations, as well as misalignments and structural deviations of components on the optical bench, also contribute to TTL coupling noise. Wegener *et al.*[13] developed a linear model using center-of-mass calibration to estimate TTL coupling, enabling spacecraft tracking. Sasso *et al.*[14–16] analyzed coupling between wavefront errors and jitter, coupling between misalignments and aberrations of the interfering wavefronts, and coupling between telescope jitter and wavefront aberrations, these researches further enriched the relevant studies on TTL coupling noise in scientific interferometer. Cui *et al.*[17] studied telescope alignment errors, finding mirror distance tolerances critical, especially between primary-secondary mirrors. Tao *et al.*[18] applied Zernike polynomials to analyze how wavefront errors affect TTL coupling and gravitational wave detection sensitivity. Wang *et al.*[19] used least-squares estimation with laser ranging data, identifying pointing angle noise as the main accuracy limitation. Li *et al.*[20] created a sensitivity matrix linking manufacturing errors to TTL coupling using Zernike polynomial analysis. Zhao[10] conducted a systematic investigation of TTL coupling noise in inter-satellite laser interferometric links under on-orbit temperature gradient conditions.

The aforementioned research shows that the TTL coupling noise factors in the scientific interferometer are numerous. However, current research requires enhancements in the following three aspects: (i) linear models fail to capture nonlinear coupling effects, (ii) individual parameter analyses cannot resolve complex system-level interactions, and (iii) the lack of comprehensive parameter sensitivity hinders design optimization. To better understand the complex interactions between these influencing parameters and TTL coupling noise, we conducted numerical simulations and developed a hierarchical model that resolves both linear correlations and nonlinear interdependencies. Through sensitivity analysis, we identify the critical parameters of the interferometer, which are most influential in the system's performance. This analysis not only aids in unraveling the noise characteristics but also provides valuable insights for the optimization of the interferometer.

2. Basic theory

To establish a consistent and physically grounded simulation model, we first outline the fundamental assumptions. Given the nature of the space-based gravitational wave detection system and its operating environment, beams are treated as a classical electromagnetic wave governed by Maxwell's equations, propagating in vacuum with a refractive index of 1. The optical system is linear and is modeled using a combination of wave optics and geometric optics.[21] Beam propagation is described using the ABCD matrix formalism under the paraxial approximation, which is valid due to the small beam divergence angles and optical component tilts.

The local reference beam emitted from a polarization-maintaining fiber is modeled as fundamental mode Gaussian beam. The complex amplitude of the electric field is given by

$$E(\boldsymbol{r},z)=E_0(z)\exp\left\{-\mathrm{i}\phi_{\mathrm{ac}}+\mathrm{i}\eta(z)-\mathrm{i}\frac{k}{2}\boldsymbol{r}^{\mathrm{T}}Q\boldsymbol{r}\right\}, \tag{1}$$

where $E_0(z)$ represents the normalization constant,φ_{ac} represents the accumulated phase, $\eta(z)$ represents the Gouy phase, k represents the wavenumber, Q represents the complex radius of the curvature tensor for generalized Gaussian beams, and the superscript T means transposed.

The Gaussian beam emitted from the fiber on the distant spacecraft propagates over millions of kilometers before being truncated by the receiving telescope on the local optical bench. At such large distances, the intensity and phase variances of the measurement beam at the telescope aperture become negligible (on the order of 10^{-30}), justifying its approximation as an ideal top-hat beam.[12]

Imperfect imaging can introduce wavefront aberration ΔZ. The complex electric field amplitude of the top-hat beam after receiving by the telescope can be expressed as[12,21]

$$E_{\mathrm{TH}}(r,z)=\begin{cases}\sqrt{\dfrac{P_{\mathrm{TH}}}{\pi}}\cdot\dfrac{1}{R_{\mathrm{TH}}}\exp\{\mathrm{i}(kz-wt+\varphi+\Delta Z)\}, & r\le R_{\mathrm{TH}},\\ 0, & r\ge R_{\mathrm{TH}},\end{cases} \tag{2}$$

where R_{TH} is the radius of the telescope, P_{TH} is the power of the top-hat beam, and φ is the phase of the beam. ΔZ is represented using Fringe–Zernike aberrations:[22]

$$\Delta Z=\sum_{i}^{N}a_i z_i, \tag{3}$$

where a_i is the coefficient of the i-th Zernike polynomial, and z_i represents the i-th Zernike polynomial.

After the top-hat beam passes through the telescope system and undergoes beam contraction, the beam transmission model based on q-parameter cannot be directly applied. Therefore, a diffraction propagation model is used to decompose the wavefront into a superposition of Hermite–Gaussian (HG) modes, approximating the actual wavefront using a finite number of modes:[21,23]

$$E_{\infty}(x,y):=\sum_{m=0}^{\infty}\sum_{n=0}^{\infty}a_{mn}\mathrm{HG}_{mn}(x,y;w_{0\mathrm{d}}), \tag{4}$$

$\mathrm{HG}_{mn}()$ denotes the Hermite polynomial, $w_{0\mathrm{d}}$ is the beam waist radius of the Hermite–Gaussian mode. The decomposition coefficient a_{mn} represents the inner product between the mode and the wavefront:[21]

$$a_{mn}=\iint\mathrm{HG}^{*}_{mn}(x,y,w_{0\mathrm{d}})E(x,y)\,\mathrm{d}x\,\mathrm{d}y. \tag{5}$$

Heterodyne measurements typically use quadrant photodiodes (QPD) with four photosensitive segments. The longitudinal pathlength signal (LPS) is then calculated by combining these outputs, as defined in LISA Pathfinder (LPF):[9]

$$\mathrm{LPS}_{\mathrm{LPF}} = \frac{1}{k}\arg(C_{\mathrm{A}} + C_{\mathrm{B}} + C_{\mathrm{C}} + C_{\mathrm{D}}), \tag{6}$$

where A, B, C, and D represent the four quadrants of the QPD.

The TTL coupling noise is characterized using the LPS, incorporating both geometric and non-geometric factors, which can be expressed as follows:[24]

$$\mathrm{LPS} = \mathrm{OPD} + \mathrm{LPS}_{\mathrm{ng}}, \tag{7}$$

where optical path length difference (OPD) represents the geometric TTL coupling noise and $\mathrm{LPS}_{\mathrm{ng}}$ represents the non-geometric TTL coupling noise. The geometric factors OPD include the lever arm effect and piston effect.[25] The lever arm effect describes the change in the geometric path length when one beam is tilted around a pivot point. The piston effect refers to the longitudinal displacement of the reflective surface caused by a tilt in the test mass (or mirror), resulting from an offset between the pivot point and the surface. The nongeometric TTL coupling noise, $\mathrm{LPS}_{\mathrm{ng}}$, encompasses the beam offset, beam parameters, signal definition, wavefront errors, and detector parameters.[24]

3. Methodology

This section models the heterodyne interference process and the signal readout of the science interferometer, while simulating TTL coupling noise to generate a database. A hierarchical model is then employed to capture the nonlinear relationships between the parameters and the noise, as well as to conduct sensitivity analysis.

3.1. Simulation model

The high-precision laser interferometric systems for space gravitational wave detection are composed of several optical components, including lasers, detectors, telescopes, beamsplitters, and mirrors. An ideal science interferometer was established based on the preliminary design of the interferometer for Taiji program,[26] as shown in Fig. 1, to simulate and analyze the TTL coupling noise. The coordinates and normal vectors of the optical components are provided in Table 1, the coordinates of RB and MB represent the origins of the two beams.

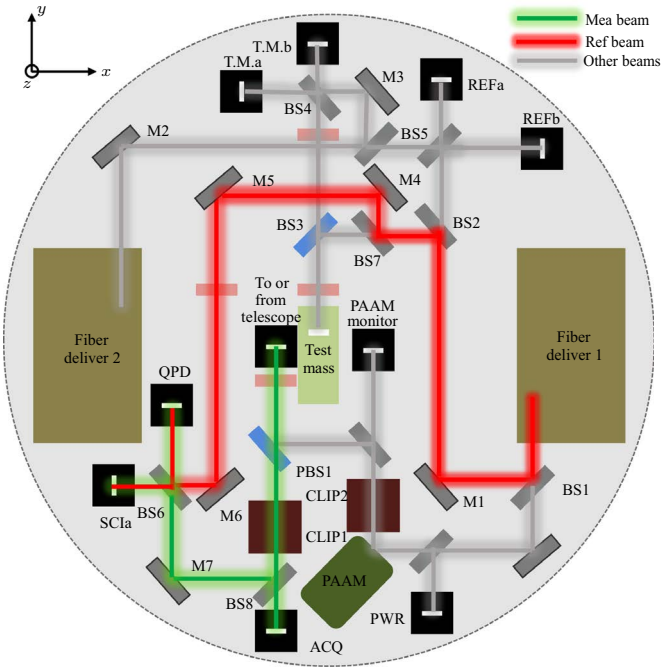


Fig. 1. Schematic diagram of the science interferometer.[26] The beam shown in red is the reference beam used for the science interferometer, while the green beam serves as the measurement beam. Beam for other interferometers, shown in grey. The gray circular base is an optical bench with the center point of the test mass as the coordinate origin and the stage normal vector as the z-axis. Its x and y-axes are shown in the upper left of the figure solely to indicate direction. The reference beam is emitted from fiber deliver 1 (F1), reflected by beam splitter 1 (BS1), mirror 1 (M1), beam splitter 2 (BS2), beam splitter 7 (BS7), mirror 4 (M4), mirror 5 (M5), mirror 6 (M6), beam splitter 6 (BS6), and finally reaches the QPD. The measurement beam is received by telescope (TS), reflected by beam splitter 8 (BS8), mirror 7 (M7), and then reaches the QPD through beam splitter 3 (BS3), and beam splitter 4 (BS4), interfering with the reference beam.

Table 1. List of the optical components of the test mass interferometer.

Item		Center coordinates			Normal vector coordinates		
Abbreviations	Description	x	y	z	x	y	z
F1	fiber deliver 1	117.4	0.5	0	0	–1	0
M1	mirror 1	66.3	–69.3	0	$\sqrt{2}/2$	$\sqrt{2}/2$	0
BS1	beam splitter 1	103.2	–69.3	0	$-\sqrt{2}/2$	$\sqrt{2}/2$	0
BS2	beam splitter 2	66.3	43.9	0	$-\sqrt{2}/2$	$-\sqrt{2}/2$	0
BS7	beam splitter 3	34.6	43.9	0	$\sqrt{2}/2$	$\sqrt{2}/2$	0
M4	mirror 4	34.6	67.2	0	$-\sqrt{2}/2$	$-\sqrt{2}/2$	0
M5	mirror 5	–53.5	67.2	0	$\sqrt{2}/2$	$-\sqrt{2}/2$	0
M6	mirror 6	–53.5	–67.5	0	$-\sqrt{2}/2$	$\sqrt{2}/2$	0
BS6	beam splitter 3	–73.9	–67.5	0	$\sqrt{2}/2$	$\sqrt{2}/2$	0
TS	telescope	–23.4	–10.2	33	0	0	–1
BS8	beam splitter 8	–23.4	–116.2	0	$-\sqrt{2}/2$	$\sqrt{2}/2$	0
M7	mirror 7	–73.9	–116.2	0	$\sqrt{2}/2$	$\sqrt{2}/2$	0
MB	measurement beam	–23.4	–10.2	0	0	–1	0
RB	reference beam	103.2	0	0	0	–1	0
QPD	quadrant photodiodes	–73.9	–30.4	0	0	–1	0

The telescope, mounted ahead of the optical bench, captures the incident beam and transmits it to the receiving port on the optical bench, as illustrated in Fig. 2.

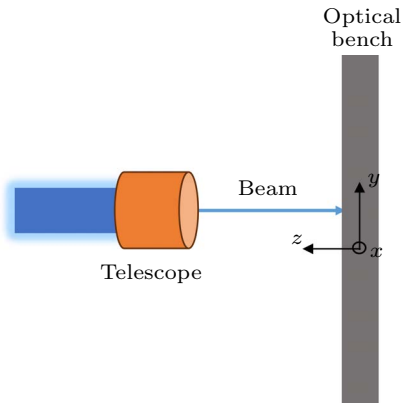


Fig. 2. Relative position of telescope and optical bench.

We comprehensively analyzed the factors influencing TTL coupling noise, then designed and simulated the heterodyne interference process within the science interferometer to accurately calculate its signal output. To improve model tractability and computational efficiency, several physical processes are idealized. Specifically, power losses during beam propagation, such as absorption, scattering, and reflection, are neglected, assuming ideal lossless transport. All optical components are modeled as ideal surfaces; only wavefront aberrations are explicitly introduced, while surface roughness and material inhomogeneities are not considered.

The simulation workflow is shown in Fig. 3. First, the simulation start time and step size are set. Then, the parameters of the optical bench are configured. TTL coupling noise is introduced by altering the telescope radius, wavefront aberrations, beam jitter angles, the position and orientation of mirrors or beamsplitters. The measurement and reference beams are modeled as a top-hat beam and a fundamental Gaussian beam characterized by the q-parameter. The top-hat beam with wavefront distortion is decomposed into a set of Hermite–Gaussian modes. The beams are traced through the interferometer components, with their propagation governed by the q-parameter transformation according to the ABCD law for paraxial optical systems. The complex electric field amplitude due to heterodyne interference is calculated. Finally, the LPS is extracted using Eq. (6).

This approach simplifies the complex system and enables more efficient TTL coupling noise analysis. Based on the aforementioned simulation, a dataset for analyzing TTL coupling noise in the science interferometer is generated. The first step involves constructing the input parameter space based on analysis level. The second step sets the value ranges and sampling intervals for each parameter, utilizing the Latin hypercube sampling method to generate 10^4 distinct input parameter combinations. Finally, the simulation is executed to obtain the corresponding LPS values for each set of input parameters.

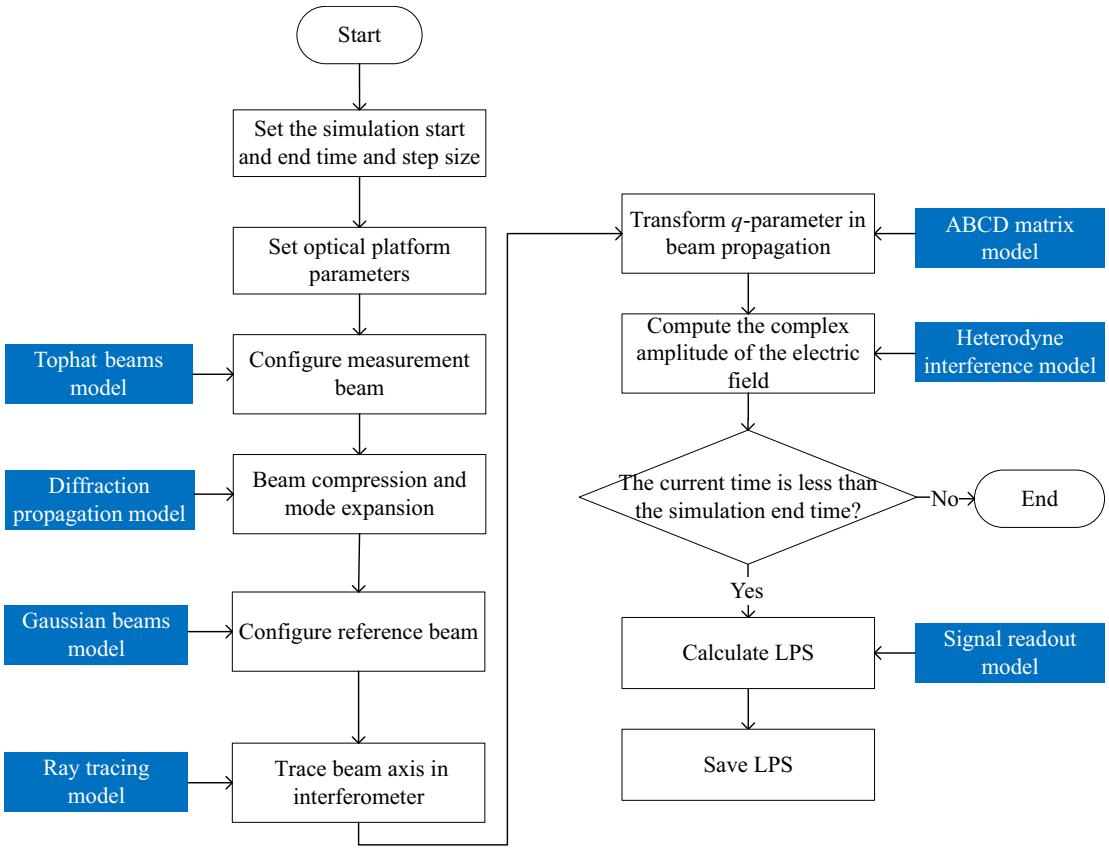


Fig. 3. Simulation flowchart of the science interferometer output.

3.1.1. Hierarchical model

The analysis of the science interferometer is conducted using a hierarchical approach for two primary reasons. First, the telescope plays a critical role as the key optical component of the science interferometer. It not only receives the incoming beam but also magnifies the angular deviations of the beam as they exit the pupil, with the amplification being inversely proportional to the beam focusing ratio.[9] Moreover, in practical designs, telescopes are never perfect; various optical aberrations, such as spherical aberration, chromatic aberration, and astigmatism, can degrade their performance. These aberrations, resulting from manufacturing imperfections, misalignments, and thermal fluctuations, can introduce distortions in the wavefront, further complicating the optical characteristics of the system. Given that the telescope itself involves about 20 parameters, it has a significant impact on the overall system performance.

Moreover, the interferometer system is characterized by a large and complex set of parameters. These parameters span a wide range of types, including pointing jitter, telescope, and wavefront aberration parameters, optical mirror parameters, and detector parameters. The diversity and sheer number of these parameters make it impractical to analyze them collectively within a single framework.

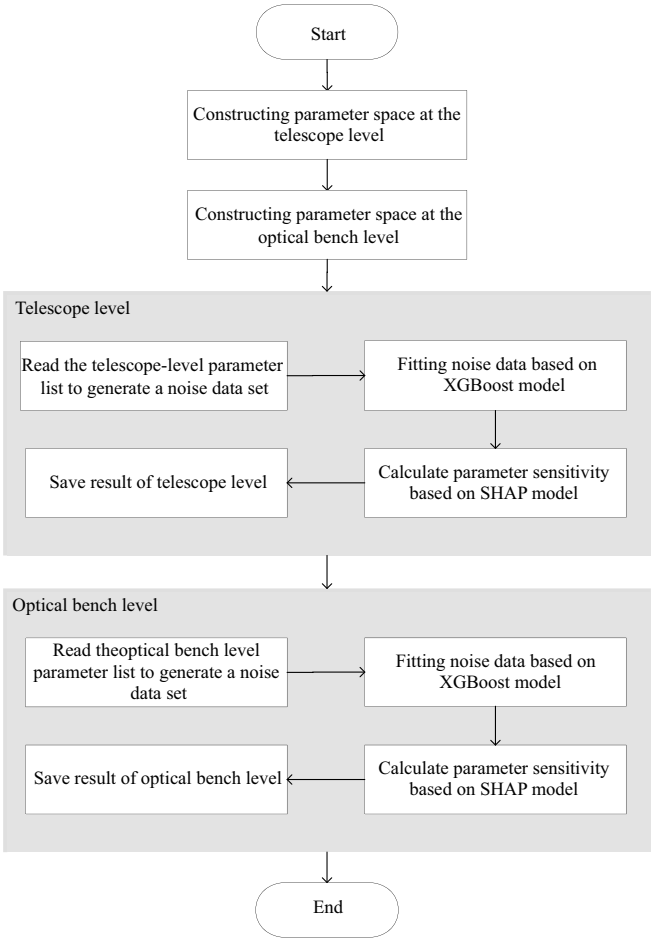


Fig. 4. Algorithmic framework for the hierarchical approach.

Given the large parameter space and the telescope's critical role, we adopt a hierarchical analysis approach. The algorithm framework of hierarchical approach is shown as Fig. 4. This method systematically divides the analysis into two levels: the telescope and the optical bench. At each level, TTL coupling noise is computed, and a machine learning model is applied to fit the relationship between parameters and noise, followed by the calculation of global parameter importance and interaction effects using attribution values. Such a division enhances the clarity of understanding the individual contributions of each component to the overall system performance.

This study employs the XGBoost (eXtreme Gradient Boosting) regression model,[27] a typical gradient boosting machine learning framework, to model the relationship between influencing parameters and LPS, aiming to address the multi-parameter coupling characteristics of TTL coupling noise. Moreover, XGBoost is well-suited for handling high-dimensional parameter problems and offers high accuracy, making it an effective tool for this analysis. XGBoost model provides feature importance values like gain, cover, and weight, but these methods have limitations and often lack interpretability. Among popular attribution methods, SHAP is the only one that is consistent and locally accurate.[28] Sensitivity analysis of the parameters is performed based on SHAP values and the SHAP attribution matrix.

The objective function of XGBoost is defined as[27]

$$\text{obj} = \sum_i l(\text{LPS}_i^{\text{pred}}, \text{LPS}_i^{\text{truth}}) + \sum_t \Omega(f_n), \tag{8}$$

where $\text{LPS}_i^{\text{pred}}$ is the predicted LPS, $\text{LPS}_i^{\text{truth}}$ is the true LPS according to the data, i is the i-th sample. l is the loss function, indicating the error between the real and predicted values, N is the number of leaves, f_n is the n-th tree, $\Omega(f_n)$ indicates the complexity of the tree; the smaller this value is, the less complex the tree and the stronger the generalization ability of the model.

The coefficient of determination R^2 is a commonly used evaluation metric in regression models, measuring the model's ability to explain the variability of the data. Its value ranges from 0 to 1, with a higher value indicating a better fit of the model to the data. R^2 reflects the model's prediction accuracy by comparing the error between predicted and actual values:

$$R^2 = 1 - \frac{\sum_i (\text{LPS}_i^{\text{pred}} - \text{LPS}_i^{\text{truth}})^2}{\sum_i (\text{LPS}_i^{\text{truth}} - \overline{\text{LPS}})^2}, \tag{9}$$

where $\overline{\text{LPS}}$ represents the average value of the LPS in the dataset.

The Shapley additive explanation (SHAP) values,[28,29] are used to interpret model predictions based on cooperative game theory. For a machine learning model with input parameters, SHAP values assess each parameter's contribution by

evaluating its marginal contribution, or the impact on the output when a parameter is excluded. SHAP synthesizes these contributions by weighing all possible parameter combinations.

The global importance based on SHAP value is calculated as follows:[28,29]

$$I_m = \frac{1}{W}\sum_{W}\left|\sum_{S\subseteq N\setminus\{m\}}\frac{|S|!(M-|S|-1)!}{M!} \times [f_x(S\cup\{m\})-f_x(S)]\right|, \tag{10}$$

where W is the number of samples, w is the w-th sample, M is the number of input parameters, m is the m-th noise influence parameter, S is the input parameter subset without m used in the XGBoost model, N is the set of all input parameters. The fractional term within the summation symbols represents the weight of the subset S, while the expression in square brackets denotes the marginal contribution of parameter m, $f_x(S)$ refers to the expected value of the function f, conditioned on the subset S of the input parameters. The LPS predicted by the XGBoost model is used as $f_x(S)$ to apply SHAP values in assessing the contribution of input parameters to TTL coupling noise.

A matrix of attribution values represent the impact of all pairs of input parameters on the predicted value of LPS:[28]

$$\begin{bmatrix} \phi_{1,1} & \phi_{1,2} & \cdots & \phi_{1,M} \\ \phi_{2,1} & \phi_{2,2} & \cdots & \phi_{2,M} \\ \vdots & \vdots & \ddots & \vdots \\ \phi_{M,1} & \phi_{M,2} & \cdots & \phi_{M,M} \end{bmatrix}. \tag{11}$$

The elements in the matrix include both interaction effects and main effects, collectively referred to as interaction values. The off-diagonal values $\phi_{m,n}$ of the matrix represents the interaction effects. The values $\phi_{m,m}$ on the diagonal represent the main effects of the parameters.

To evaluate the statistical significance of SHAP value rankings, this study employs Kendall's coefficient of concordance (Kendall's W) to quantitatively assess ranking stability. The coefficient is calculated as

$$W = \frac{12S_{\mathrm{p}}}{k^2(n_{\mathrm{p}}^3-n_{\mathrm{p}})}, \tag{12}$$

where S_{p} represents the sum of squared deviations between each parameter's rank sum and the mean rank sum, K denotes the number of samples, and n_{p} is the total number of parameters. The statistic ranges from 0 to 1, with values approaching 1 indicating perfect agreement among rankings.

The analysis procedure consists of 3 key steps. First, 30 bootstrap subsamples are generated to compute SHAP values and record parameter rankings. Second, Kendall's W coefficient is calculated across all rankings, followed by hypothesis testing ($H_0: W = 0$; $H_1: W > 0$, $p = 0.05$). Rejection of H0 when the test result is $p < 0.05$ confirms the statistical significance of ordering stability. This rigorous validation addresses potential instability concerns in interpretable machine learning applications.

4. Results and discussion

4.1. Parameter settings

According to the science interferometer shown in Fig. 1, the parameters of the telescope level are divided into two categories: pointing jitter parameters and telescope parameters. The optical bench parameters are divided into three categories: beam parameters, mirror and beam splitter parameters, and QPD parameters. The parameter range refers to the index requirements of Taiji-3.[10,30,31]

The categories, parameters, and ranges of the telescope-level parameters and optical bench level parameters are listed in Tables 2 and 3. Due to the presence of non-conservative forces in space, relative satellite displacements can induce angular deviations in the measurement beams, resulting in three-dimensional pointing jitter of the measurement beam. The telescope system under investigation is characterized by several key parameters, including entrance pupil radius, exit pupil radius, and their modulation effects on the incident wavefront. Since the measurement beam parameters couple with the telescope's optical characteristics during propagation, they are integrated into the telescope-level parameter space. These aberrations primarily originate from manufacturing imperfections, assembly errors, and thermal fluctuations. The telescope's optical properties are quantitatively described using Zernike polynomials, specifically including the following 15 terms: piston, tilt x, tilt y, defocus, astigmatism x, astigmatism y, coma x, coma y, primary spherical, trefoil x, trefoil y, second astigmatism x, second astigmatism y, tetra foil x, and tetra foil y. A total of 20 parameters made up the telescope-level parameter space simulated and analyzed in this paper.

Table 2. Telescope-level parameter information for the simulation and analysis of TTL coupling noise.

Categories	Parameters	Ranges
Measurement beam parameter	angle of measurement beam	(9 nrad, 11 nrad)
	wavelength	1064 nm
Telescope parameters[4]	entrance pupil radius	(199 mm, 201 mm)
	exit pupil radius	(1.99 mm, 2.01 mm)
	piston	(0 nm, 1 nm)
	tilt x, tilt y	(1 nrad, 2 nrad)
	wavefront aberration	$\lambda/30$

Table 3. Optical bench level parameter information for the simulation and analysis of TTL coupling noise.

Categories	Parameter	Range
Reference beam parameters	waist radius	(0.4 mm, 0.6 mm)
	waist position	(−1 cm, 1 cm)
	beam offset	(−10 μm, 10 μm)
Mirror and beam splitter parameters	rotation point offset	(−10 μm, 10 μm)
	angle	(−75 μrad, 75 μrad)
QPD parameters	radius	(599.8 μm, 600.2 μm)
	slit size	(9.8 μm, 10.2 μm)

The beam parameters include the waist radius and waist position of the reference beam. The optical components in an ideal science interferometer are mainly beam splitters and mirrors. The displacement and deflection of these components caused by in-orbit temperature and gravity release will cause TTL coupling noise.[10,12] The QPD parameters include the radius and slit size. A total of 66 parameters made up the optical bench level parameter space simulated and analyzed in this paper.

4.2. Results of parameter sensitivity analysis

According to the defined parameter space for each level, the XGBoost model is used to predict the LPS value caused by TTL coupling noise, and sensitivity analysis is performed by calculating the global importances.

The global importance of key parameters at the telescope level, calculated based on SHAP values, is shown in Table 4. The variable definition rule is as follows: 'y_{a}' before the underscore denotes the angle of rotation around the y-axis, while 'tophat' after the underscore refers to the top-hat beam. 'R' represents the radius, 'TS1' refers to the telescope's entrance pupil, and 'TS2' refers to the telescope's exit pupil.

Table 4. The global importances for telescope-level influencing factors of TTL coupling noise.

Variable	Meaning	Global importance
$y_{\mathrm{a_tophat}}$	angle of measurement beam (y-axis)	0.456
$x_{\mathrm{a_tophat}}$	angle of measurement beam (x-axis)	0.447
R_{TS1}	entrance pupil radius	0.048
R_{TS2}	exit pupil radius	0.048

A higher sensitivity indicates that parameter variations have a greater impact on TTL coupling noise, highlighting the importance of these parameters during instrument design. At the telescope level, the angle of the measurement beam with respect to the y-axis and x-axis demonstrates the most significant impact on noise, with global importance scores of 0.456 and 0.447, respectively. The next most influential parameters are the entrance and exit pupil radius, each with a global importance of approximately 0.05. Pointing jitter is affected by two main factors: first, the relative misalignment between spacecraft, which causes angular deviations in the measurement beam; and second, the beam compression, which magnifies the jitter angle inversely according to the compression ratio. When a top-hat beam with angular deviation propagates through the interferometer bench, it induces both the lever arm effect and beam displacement on the QPD, generating TTL coupling noise. The sensitivity analysis reveals that the impacts of the entrance and exit pupil radii are comparable. The telescope radius is influenced by manufacturing errors and temperature variations. Based on this analysis, maintaining the relative stability of spacecraft positions and carefully choosing materials and controlling temperature within the telescope are crucial for minimizing TTL coupling noise.

To further elucidate these results, we introduce a simplified analytical model. Phase fluctuations arising from laser pointing jitter are known to contribute to the tilt-to-length coupling noise in precision interferometry, with their functional form given by[32]

$$\delta\phi = \frac{1}{32}\left(\frac{2\pi}{\lambda}\right)^3 \mathrm{d}D^2\theta_{\mathrm{dc}}\delta\theta, \tag{13}$$

where θ_{dc} represents the static pointing offset, $\delta\theta$ denotes pointing jitter, and D is the telescope aperture diameter.

Considering thermal effects, the telescope's diameter exhibits temporal variations due to thermal expansion/contraction of the materials. Crucially, the beam angle magnification factor is determined by the ratio between the receiving and output diameters. Consequently, any thermally-induced diameter variation modulates the pointing jitter proportionally. The resulting temperature-dependent phase noise can therefore be formulated as

$$\delta\phi' = \frac{1}{32}\left(\frac{2\pi}{\lambda}\right)^3 \mathrm{d}D^2(t)\theta_{\mathrm{dc}}m\delta\theta, \tag{14}$$

where $D(t)$ represents the thermally-induced diameter variation, $m\delta\theta$ corresponds to the temperature-dependent pointing jitter modification. m is the amplification factor of the angular jitter introduced by the telescope's magnification ratio. The analytical results establish that by controlling material properties and thermal stability to suppress thermally-induced pupil diameter variations, beam pointing fluctuations can be effectively regulated, leading to significant TTL coupling noise reduction.

The global importance of key parameters at the optical bench level, calculated based on SHAP values, is shown in Table 5. The angles of mirror or beamsplitter around z-axis have the greatest impact on TTL coupling noise at optical bench

level, with a global importance of approximately 0.1. Numerically, the sensitivity of the parameters for each mirror is consistent, and the order of beam propagation does not affect this sensitivity. Due to in-orbit temperature fluctuations and gravitational release, mirrors and beamsplitters experience dynamic random jitter, which induces the lever arm effect, piston effect and beam displacement on the QPD. Therefore, selecting appropriate materials for optical components and maintaining precise temperature control are critical for effectively mitigating TTL coupling noise.

Table 5. The global importances for optical bench level influencing factors of TTL coupling noise.

Variable	Meaning	Global importance
$z_{\text{a_M1}}$	angle of M1 (z-axis)	0.122
$z_{\text{a_BS1}}$	angle of BS1 (z-axis)	0.120
$z_{\text{a_BS8}}$	angle of BS8 (z-axis)	0.111
$z_{\text{a_BS2}}$	angle of BS2 (z-axis)	0.111
$z_{\text{a_BS7}}$	angle of BS7 (z-axis)	0.104
$z_{\text{a_BS6}}$	angle of BS6 (z-axis)	0.090
$z_{\text{a_M7}}$	angle of M7 (z-axis)	0.087
$z_{\text{a_M5}}$	angle of M5 (z-axis)	0.086
$z_{\text{a_M4}}$	angle of M4 (z-axis)	0.084
$z_{\text{a_M6}}$	angle of M6 (z-axis)	0.082

As shown in Fig. 5, the telescope-level SHAP interaction value rankings exhibit exceptional consistency (Kendall's $W = 0.826$, $p = 0.013$), indicating statistically significant agreement. Each row represents 10^4 data points, corresponding to the sample size of the dataset. The colors of the data points correspond to different effects, with red indicating a positive change in the parameter and blue indicating a negative change. Main effects are displayed for individual parameters, while interaction effects are shown when parameters are considered together. For instance, when $y_{\text{a_tophat}}$ is displayed alone, it represents the main effect of the measurement beam angle (y-axis). However, when $y_{\text{a_tophat}} - \langle\text{other parameters}\rangle$ is shown, it illustrates the interaction effect between $y_{\text{a_tophat}}$ and other parameters, capturing the combined influence on TTL coupling noise. The width of the plot reflects the concentration of data samples, with wider subplots indicating a greater impact on noise, both for main and interaction effects. Figure 6 presents the SHAP interaction value strength at the telescope level, quantifying the proportional contribution of parameter interactions to the total noise. The plots clearly demonstrates that the pointing jitter angle of measurement beam has a significant impact on TTL coupling noise. In addition to the substantial effect of individual parameters, the interaction between angles of measurement beam also contributes to TTL coupling noise. Therefore, when aiming to suppress TTL coupling noise, particular attention should be given to the pointing jitter, which serves as a critical design constraint for the relative stability between satellites.

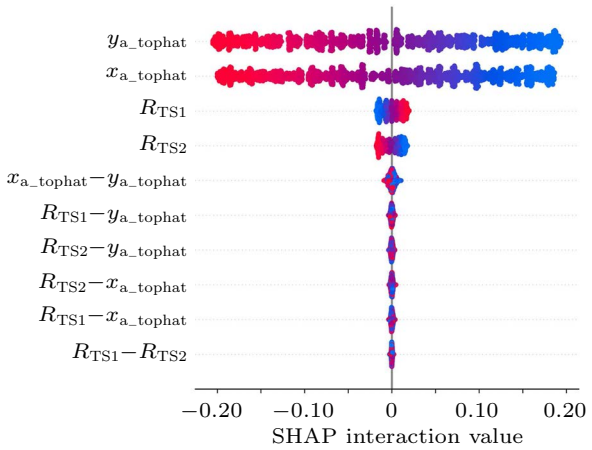


Fig. 5. Ranking of SHAP interaction values for telescope-level. The left side of the figure shows the parameters or interaction parameters, with the main effects or interaction effects arranged in descending order from top to bottom.

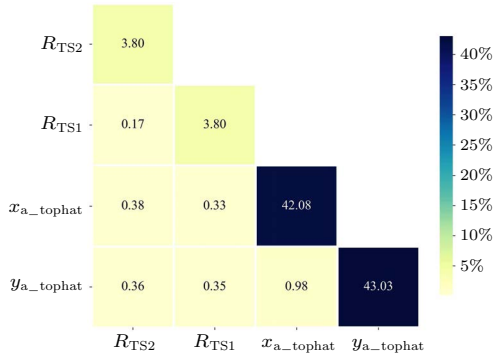


Fig. 6. Heatmap of the strength of telescope-level SHAP interaction values.

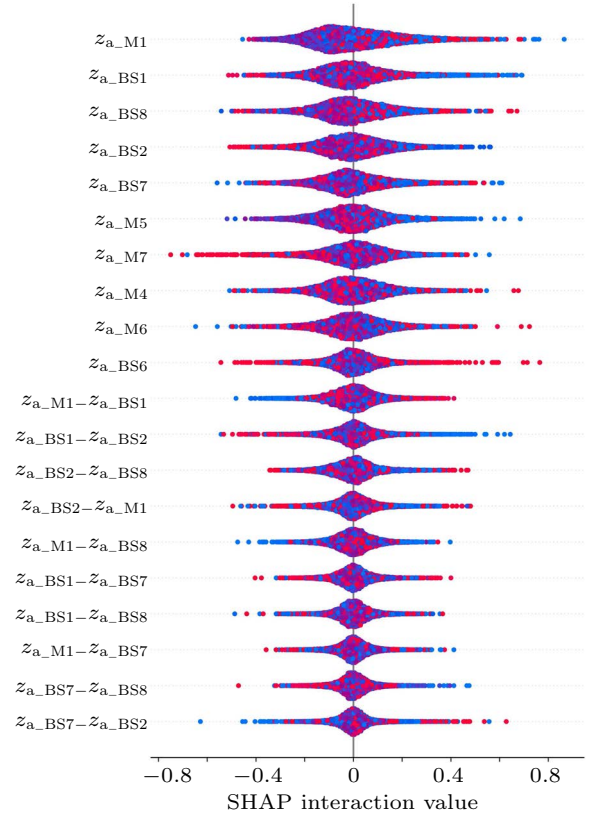


Fig. 7. Ranking of SHAP interaction values for optical bench level.

Figure 7 shows the ranking of the SHAP interaction values at the optical bench level. At the optical bench level, the SHAP interaction value rankings demonstrated robust consistency, with Kendall's W coefficient reaching 0.760 ($p = 0.39$), indicating statistically significant agreement. Figure 8 presents the SHAP interaction value strength at the optical bench level. It is obvious from the figures that the angle of the mirror and beam splitter along the z-axis has a strong effect on the TTL coupling noise. In addition to the strong influence of individual parameters on TTL coupling noise, the interaction between different mirror angles also contributes to TTL coupling noise. Therefore, special attention should be given to the angle around z-axis when suppressing TTL coupling noise. This provides constraints for the selection of optical component materials and temperature control on the optical bench.

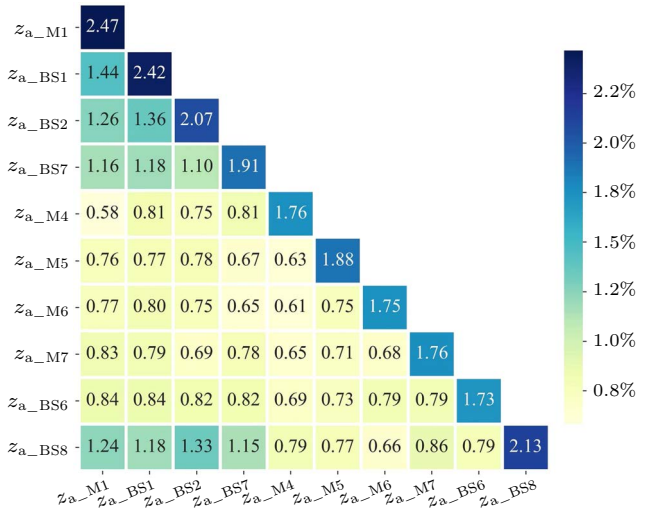


Fig. 8. Heatmap of the strength of optical bench-level SHAP interaction values.

After retaining the top 3 and top 10 parameters for each level, the R-squared value stabilizes around 0.8, indicating that the XGBoost model effectively fits the relationship between key parameters and TTL coupling noise, even after eliminating redundant ones.

5. Conclusion

Based on Gaussian beams, top-hat beams, diffraction propagation, ray tracing, ABCD matrices, heterodyne interference, and QPD signal readout models, simulations of the Taiji program's science interferometer were conducted at both the telescope and optical bench levels to generate TTL coupling noise data. Sensitivity analysis was conducted for single-factor and multi-factor scenarios by combining SHAP values with attribution matrices. This analysis reduced the parameter space from 20 dimensions to 4 dimensions at the telescope level, retaining key parameters including pointing jitter angles, telescope entrance pupil radius, and exit pupil radius. Similarly, the optical bench level parameter space was reduced from approximately 66 dimensions to 10 dimensions, focusing primarily on angle-related parameters.

At the telescope level, the analysis revealed that pointing jitter angles around the y- and x-axes had the greatest impact on TTL coupling noise, followed by the telescope's entrance and exit pupil radii. Additionally, the interaction between pointing jitter and the telescope radius also contributed to the noise. At the optical bench level, z-axis angles of mirrors and beamsplitters showed the strongest effects on TTL coupling noise, with interactions between these angles playing an important role. These results suggest that future experiments should prioritize parameters related to pointing jitter and telescope radius, while also focusing on angular jitter of optical components on the interferometer bench.

This study presents a hierarchical sensitivity analysis framework to systematically investigate and quantify the dominant factors influencing TTL coupling noise in the scientific interferometer system. The analysis yields critical design constraints across multiple subsystems: (i) required stability specifications for satellite relative positioning, (ii) optimal material selection and thermal control parameters for the telescope assembly, and (iii) temperature management for the optical bench components. Furthermore, the proposed methodology successfully addresses computational convergence challenges associated with high-dimensional parameter optimization ($N = 86$), demonstrating robust performance in identifying key parameters while maintaining numerical stability. This systematic approach provides an effective optimization strategy for complex interferometer systems, achieving an 84% reduction in parameter space dimensionality without compromising analytical accuracy.

Looking forward, future research can focus on several promising directions to enhance the applicability and robustness of the current framework. First, incorporating more detailed physical modeling of the telescope and optical bench components, including realistic surface imperfections, thermal-mechanical coupling, and in-orbit environmental effects, would improve the fidelity of simulations and better capture subtle noise sources. Second, expanding the dataset with experimental or on-orbit measurement data will enable more accurate calibration and validation of the machine learning models, further enhancing the physical interpretability of sensitivity results. Third, integrating causal inference techniques alongside XGBoost and SHAP could provide deeper insights into the underlying physical mechanisms governing TTL coupling noise, moving beyond correlation-based analysis. Lastly, exploring adaptive sampling and active learning methods may reduce the computational burden of high-dimensional simulations, enabling real-time or near-real-time sensitivity analysis for evolving mission conditions. These developments will significantly broaden both the theoretical boundaries and practical applicability of the proposed method, providing valuable

guidance for designing and operating future space-based gravitational wave detectors.

Appendix A

To assess the appropriate decomposition order for Hermite–Gaussian modes, this study employs the normalized mean squared error (NMSE) as the quantitative evaluation metric. The NMSE is calculated as

$$\mathrm{NMSE} = \frac{\left\| E^N(x,y) - E_{\mathrm{TH}}(x,y) \right\|^2}{\left\| E_{\mathrm{TH}}(x,y) \right\|^2}, \tag{A1}$$

where $E^N(x,y)$ represents the decomposed beam with order N, and $E_{\mathrm{TH}}(x,y)$ denotes the top-hat beam with wavefront distortion. The beam parameters are specified in Table A1.

Table A1. Top-hat parameter information with wavefront aberrations.

Parameter	Value
Power	1.25×10^{-9} W
Beam radius	2 mm
Wavelength	1064 nm
Wavefront error	$\lambda/30$

The decomposition was performed for mode orders $N =$ 5, 10, 20, 30, and 40. The corresponding NMSE values are presented in Table A2. The results demonstrate that at $N = 40$, the decomposition achieves an NMSE of 1%, indicating excellent reconstruction accuracy. However, considering computational efficiency, we select $N = 20$ as the optimal order, which maintains 95% accuracy while offering significantly improved computation speed.

Table A2. Normalized mean square error at different decomposition orders.

Mode order (N)	NMSE
5	0.10
10	0.07
20	0.05
30	0.02
40	0.01

Acknowledgements

Project supported by the National Key Research and Development Program of China (Grant No. 2020YFC2200100) and the CAS's Strategic Pioneer Program on Space Science (Grant No. XDA1502110201).

References

[1] Sigg D and the LIGO Scientific Collaboration 2008 *Class. Quantum Grav.* **25** 114041
[2] Colpi M, Danzmann K, Hewitson M, Holley-Bockelmann K, *et al.* https://www.cosmos.esa.int/web/lisa/documents [2025-1-10]
[3] Chen Y and Zhu Z 2024 *Chin. Phys. B* **33** 080401
[4] Luo Z, Wang Y, Wu Y, Hu W and Jin G 2021 *Prog. Theor. Exp. Phys.* **2021** 05
[5] Luo J, Chen L, Duan H, Gong, Hu S, Ji J, Liu Q, Mei J, Milyukov V, Sazhin M, Shao C, Toth V T, Tu H, Wang Y, Wang Y, Yeh H, Zhan M, Zhang Y, Zharov V and Zhou Z 2016 *Class. Quantum Grav.* **33** 035010
[6] Otto M 2015 *Time-delay interferometry simulations for the laser interferometer space antenna* Ph.D. Dissertation (Hanover: Gottfried Wilhelm Leibniz Universität Hannover)
[7] Hu W and Wu Y 2017 *National Science Review* **4** 685
[8] Danzmann K and Team T L S 1996 *Class. Quantum Grav.* **13** A247
[9] Schuster S 2017 *Tilt-to-length coupling and diffraction aspects in satellite interferometry* Ph.D. Dissertation (Hanover: Gottfried Wilhelm Leibniz Universität Hannover)
[10] Zhao Y 2021 Ph.D. Dissertation (Beijing: University of Chinese Academy of Sciences) (in Chinese)
[11] Danzmann K, Prince T A, Binetruy P, Bender P, *et al.* https://sci.esa.int/web/lisa/-/48364-lisa-assessment-study-report-yellow-book [2025-1-10]
[12] Wang Z, Yu T, Zhao Y, Luo Z, Sha W, Fang C, Wang Y, Wang S, Qi K, Wang Y and Xu X 2020 *Photonic Sens.* **10** 265
[13] Wegener H, Müller V, Heinzel G and Misfeldt M 2020 *Journal of Spacecraft and Rockets* **57** 1362
[14] Sasso C P, Mana G and Mottini S 2018 *Class. Quantum Grav.* **35** 185013
[15] Sasso C P, Mana G and Mottini S 2018 *Class. Quantum Grav.* **35** 245002
[16] Sasso C P, Mana G and Mottini S 2019 *Opt. Express* **27** 16855
[17] Cui X, Fang C and Wang Z 2023 *Acta Optica Sinica* **43** 1
[18] Tao Y Z, Jin H B and Wu Y L 2023 *Chin. Phys. B* **32** 024212
[19] Wang Z, Yang S, Jia F, Wu K, Liao F, Duan H and Yeh H 2024 *Remote Sensing* **16** 862
[20] Li J, Lin H, Huang Y, Yu M, Luo J, Xiao Z, Wang Z and Wu Y 2023 *Meas. Sci. Technol.* **34** 055409
[21] Mahrdt C 2014 *Laser link acquisition for the GRACE follow-on laser ranging interferometer* Ph.D. Dissertation (Hanover: Gottfried Wilhelm Leibniz Universität Hannover)
[22] Genberg V L, Michels G J and Doyle K B 2002 *Optomechanical Design and Engineering*, September 9, 2002, Seattle, USA, p. 276
[23] Zhao M, Tao Y, Weber K, Kaune T, Schuster S, Hao Z and Wanner G 2023 *Sensors* **23** 9024
[24] Hartig M S, Schuster S, Heinzel G and Wanner G 2023 *J. Opt.* **25** 055601
[25] Hartig M S, Schuster S and Wanner G 2022 *J. Opt.* **24** 065601
[26] Luo Z, Guo Z, Jin G, Wu Y and Hu W 2020 *Results in Physics* **16** 102918
[27] Chen T and Guestrin C 2016 *Proceedings of the 22nd ACM SIGKDD International Conference on Knowledge Discovery and Data Mining KDD'16: The 22nd ACM SIGKDD International Conference on Knowledge Discovery and Data Mining*, August 13, 2016, San Francisco California, USA, p. 785
[28] Lundberg S M, Erion G G and Lee S I 2019 arXiv:1802.03888 [cs.LG]
[29] Borgonovo E, Plischke E and Rabitti G 2024 *European Journal of Operational Research* **318** 911
[30] Zhao M, Peng X, Yang Z, Meng X, Ma X and Zhang J 2022 *J. Astron. Telesc. Instrum. Syst.* **8** 038002
[31] Tao W, Deng X, Diao Y, Gao R, Qi K, Wang S, Luo Z, Sha W and Liu H 2023 *Sensors* **23** 9141
[32] Bender P L 2005 *Class. Quantum Grav.* **22** S339